Current filament patterns in *n*-GaAs layers with different contact geometries

J. Hirschinger, F-J. Niedernostheide,* and W. Prettl
Universität Regensburg, Institut für Experimentelle und Angewandte Physik, 93040 Regensburg, Germany

V. Novák
Institute of Physics AS CR, Cukrovarnická 10, 162 00 Praha 6, Czech Republic
(Received 14 June 1999)

In thin n-GaAs epitaxial layers current filament patterns formed by low-temperature impurity breakdown have been visualized for different contact geometries. Independent of the contact geometry, after nucleation a generic shape of filaments has been observed in the form of a stripe of high current density with parallel borders whose width is proportional to the sample current. Filament splitting processes could be attributed to geometrical properties of the contacts without any inherent critical width. In a magnetic field applied normal to the semiconductor film two different types of stable filament configurations have been found. One can be characterized by a filament deflection in the direction of the Lorentz force acting on the electrons, the other one by a filament tilting related to the Hall angle. The experimental results are explained in terms of a simple mathematical model.

I. INTRODUCTION

At low temperatures, high-purity semiconductors with a small concentration of shallow impurities exhibit an electric breakdown which is connected with a pattern formation process in the current flow. At low electric fields almost all charge carriers are bound to impurities and the material is practically insulating. Exceeding a threshold value of the electric field, the autocatalytic process of impact ionization of shallow impurities causes the current to increase avalanchelike by several orders of magnitude.[1] After breakdown two different nonequilibrium phases of drastically different conductivity coexist in the sample: a current filament connecting the contacts, which carries practically the total current, being embedded in a low-conducting environment.

So far, it is not quite clear to what extent self-organization controls the formation of macroscopic filamentary patterns. Some authors suggested that a self-organizing mechanism is involved merely in the formation of the interface between the low-conducting and the high-conducting phases, whereas the shape of the observable filaments is a problem of electrostatics.[2,3] Many experimental results published so far relate to samples with two point contacts.[2–6] This contact configuration yields relatively stable filamentary structures, but a significant influence of the inhomogeneous field between the contacts is inevitable in this case. Nevertheless, recently an analogous type of pattern formation in the regime of low-temperature breakdown has been found in contactless samples in a uniform microwave field.[7] To assess the influence of the field inhomogeneity imposed by the contacts we investigated filamentary pattern formation in four different contact geometries: a pair of point contacts, a pair of parallel stripe contacts, two concentric circular contacts with comparable radii (ring geometry), and Corbino geometry. This allows a concise comparison of filament growth and splitting processes.

In a magnetic field perpendicular to the semiconductor layer, current filaments are known to be deformed[5] and destabilized.[8–11] However, up to now no common picture of the effect of the magnetic field on current filaments has been given. Upon analyzing the symmetry of the filamentary structures in a magnetic field we discuss the possible mechanisms through which the magnetic field acts.

Furthermore, the experimental results reported here are compared to a two-dimensional numerical model based on the Drude theory of galvanomagnetic transport. In spite of its simplicity, the model is shown to yield a relevant explanation of many of the filament properties.

II. EXPERIMENTAL SETUP

The experimental method is based on the quenching of impurity and exciton luminescence under the influence of an electric field in the post breakdown regime.[6] The spatial distribution of photoluminescence reflects the density of free carriers in the semiconductor layer and filaments appear as dark stripes in images recorded with an infrared sensitive image intensifier camera. The samples were immersed in liquid helium at a temperature of 1.8 K, placed in the center of a superconducting magnet, and biased in series with a load resistor in the order of 10 kΩ.

The measurements have been carried out on several molecular beam epitaxy grown *n*-GaAs epitaxial layers with a shallow donor concentration in the order of 10^{15} cm^{-3} at about 20% compensation. The thickness of the epitaxial layers was about 3 μm. Electric contacts were prepared on samples of the material in four different geometries: two parallel stripe contacts, two distant point contacts, Corbino geometry with a central dot contact, and a concentric arrangement of two ring electrodes. Detailed material and sample properties are summarized in Table I.

III. MATHEMATICAL MODEL

We adopt the model of Ref. 13 and generalize it for case of nonzero normal magnetic field. The model is based on the

TABLE I. Sample parameters. The layer thicknesses in brackets correspond to the nondepleted parts of the epitaxial layers (Ref. 12).

	PA06	PB01	PB15	PC06	B3	C1, C5	C6
contact geometry	points	stripes	stripes	points	points	Corbino	ring
contact distance (mm)	3.05	1.65	1.05	2.15; 3.05	2.7; 4.0; 6.1	1.0	0.5
contact diameter (mm)	0.3			0.3	0.08	0.08 / 2.1	2.0 / 3.0
layer thickness (μm)	4.3 (3.6)	4.3 (3.1)	4.3 (3.1)	4.3 (2.9)	3 (2.3)	3 (2.3)	3 (2.3)
n at 77 K (10^{15} cm^{-3})	7.1	2.6	2.6	1.9	5.0	5.0	5.0
μ at 77 K (10^3 cm^2/V s)	21	41	41	43	28	28	28
j_c (A/mm^2)	0.6	0.6	0.6	0.6	0.8	0.8	0.8
$\mathcal{E}_c$ (V/cm)	10.3	7.7	7.7	6.2	8.9	9.7	9.4

following assumptions: (i) the high- and low-conducting phases are in a stationary state separated by a thin interface—the filament boundary—through which no current flows; (ii) along the interface the electric field strength equals to some constant critical value $\mathcal{E}_c$. The continuity equation $\nabla \cdot \boldsymbol{j} = 0$ for the current density $\boldsymbol{j}$ is then to be solved in a region whose boundaries are not known in advance. The boundaries must be self-consistently adjusted to meet the condition (ii) in addition to the usual boundary conditions of fixed potential on the contacts and zero normal current on the filament edges.[13] The current density $\boldsymbol{j}$ is described by the Drude model

$$\boldsymbol{j} = \frac{\sigma_0}{1+(\mu B)^2} \begin{pmatrix} 1 & -\mu B \\ \mu B & 1 \end{pmatrix} \boldsymbol{\mathcal{E}}, \tag{1}$$

where B is the magnetic field normal to the current flow, σ_0 is the conductivity of the high-conducting phase at $B=0$, μ is the electron mobility, and $\boldsymbol{\mathcal{E}}$ is the electric field vector.

The above defined free-boundary problem is solved in an iterative procedure by a finite-element method. Let us note that every solution of the problem is isotropically scalable, provided that the applied voltage or the given boundary field strength $\mathcal{E}_c$ are scaled accordingly. It should be stressed that within the presented model $\mathcal{E}_c$ is merely a phenomenological constant.

IV. FILAMENT PATTERNS IN THE MAGNETIC-FIELD-FREE CASE

Figures 1(a)–(d) show the formation of a filament in a sample with parallel stripe contacts as the sample current is increased. After the breakdown, a single filament with almost parallel borders nucleates. As the current is increased this initital filament gets broader and other filaments may also nucleate. In most cases the additional filaments appear close to the original one. In contrast to previous results,[14] no critical upper limit of the filament width related to the filament division process could be identified. Instead, filaments of any width fitting in the lateral extent of the sample have been observed, and filaments differing in width by more than an order of magnitude have been found to coexist between parallel stripe contacts. Moreover, filament splittings in each sample of this contact geometry has often been observed to occur at the same positions, which indicates that the splitting is induced by imperfections on the contacts or in the epitaxial layer.

A stripelike filament running perpendicular to the parallel contacts corresponds to a trivial solution of the above described model for $B=0$: a region with uniform electric field is split into stripes of constant finite conductivities, which follow the field lines and thus do not disturb the field distribution. As the electric field is spatially uniform, the condition (ii) of the model is met at a constant voltage bias, at which the field strength in the sample equals $\mathcal{E}_c$. It should be noted that in this case no reason for filament splitting can be found in the model. All configurations of parallel filaments are allowed, regardless of their widths.

Unlike the case of parallel stripe contacts, the electric field distribution in other contact geometries is inherently

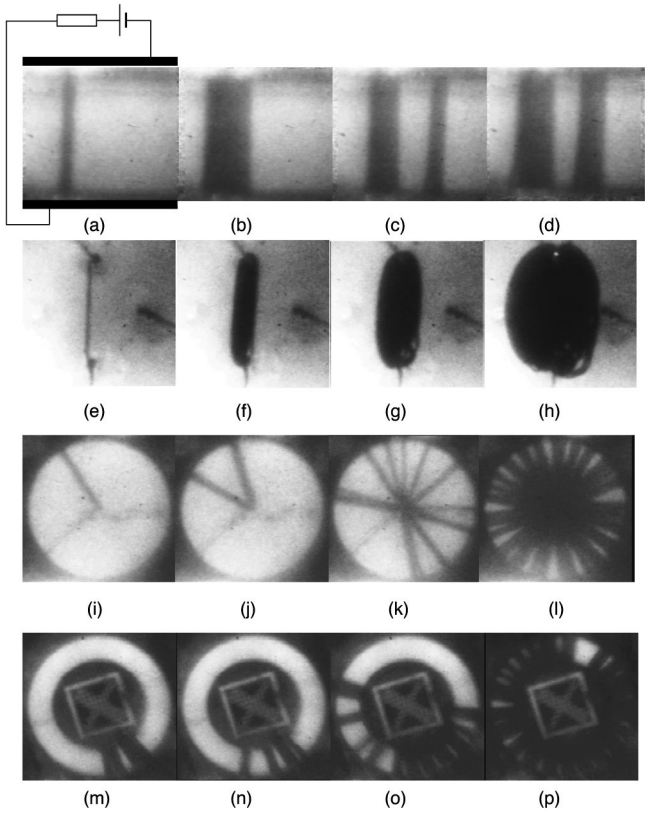

FIG. 1. Nucleation of current filaments in four different contact geometries: (a)–(d) parallel stripe contacts (sample PB01), $I = 0.25$, 1.00, 1.00, 1.35 mA; (e)–(h) two point contacts (sample PA06), $I = 0.16$, 1.62, 3.41, 10.1 mA; (i)–(l) Corbino geometry (sample C5), $I = 0.17$, 0.47, 1.71, 7.08 mA; (m)–(p) ring geometry (sample C6), $I = 1.54$, 1.58, 5.73, 13.0 mA.

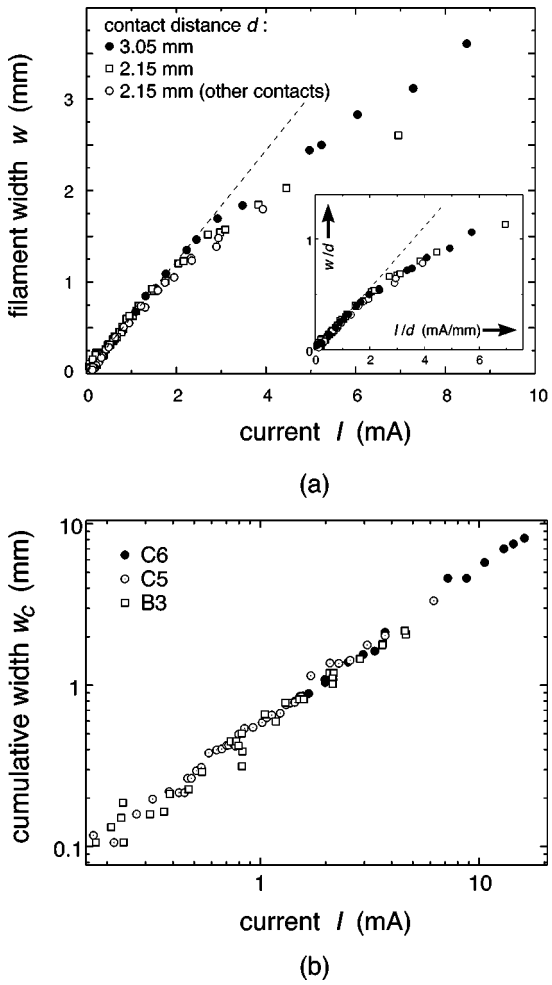

FIG. 2. (a) Dependence of filament width w on the current I between two point contacts for different contact distances (sample PC06). In the inset the dependences are normalized by the contact distance d. (b) Cumulative width $w_c=\Sigma w$ of all coexisting filaments as a function of the total sample current I between different contact geometries of the same epitaxial layer: two point contacts (B3), Corbino geometry (C5), and ring geometry (C6).

inhomogeneous. Despite this, the impurity breakdown in these cases has also been found to result in the formation of stripelike filaments with parallel borders, as can be seen in Fig. 1. The only exception to this generic behavior are filaments between two point contacts, which become distinctly convex at high currents, Figs. 1(g) and 1(h).

The transition from a parallel bordered to a convex-shaped filament between the point contacts can also be seen in the dependence of the filament width w on the current I, as shown in Fig. 2(a). As long as the filament width is small in comparison to the contact distance, the filament borders are parallel and the width increases proportionally with the current. At higher currents when the filament width becomes comparable to the contact distance the borders of the filament become more and more convex and the width increases sublinearly with the current [see Fig. 2(a)]. However, if the filament width w is normalized by the contact distance d, and the current I is scaled by the same ratio, the w vs I curves corresponding to samples with different contact distances cover exactly each other, as shown in the inset of Fig. 2(a). This fact is a strong experimental indication of a purely geometrical effect of the contact arrangement, and conforms well with the scalability of the proposed model.

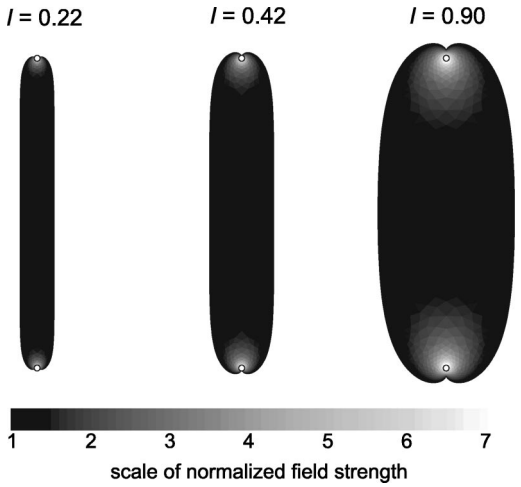

FIG. 3. Simulation results in point contact geometry for three different bias voltages. The gray scale reflects the local field strength, normalized to the critical (boundary) field. Current I is in arbitrary units.

The width of a parallel-bordered filament is proportional to the current and does not depend on the contact geometry. This is illustrated in Fig. 2(b), where the cumulative width of all the parallel-bordered filaments coexisting in a sample is plotted against the total current. It can be seen that the width rises linearly over more than two orders of magnitude. In addition, as indicated in the figure the plotted data correspond to three different contact geometries on samples of the same material. The common proportionality constant, which is in fact the critical current density j_c inside the filament, can therefore be regarded as a material parameter of the epitaxial layer. Numerical values of j_c are shown in Table I.

Assuming a constant carrier mobility μ and concentration n in the sample, the existence of the constant critical current density j_c implies a constant value of the electric field inside the filament with parallel borders. This result clearly reveals that the electric field inside the current filament is significantly redistributed in comparison to a uniformly conducting filamentless layer, where, e.g., in the Corbino sample the electric field drops with $1/r$.

The redistribution of electric field is well reproduced by the mathematical model at $B=0$. In Fig. 3 three numerical solutions are shown for various bias voltages in a sample with two point contacts. The tendency of the system to form the parallel bordered filaments with a uniform field inside is obvious. In addition, it can be shown numerically that any symmetric perturbation of the parallel bordered form relaxes exponentially. The relaxation length was found to be about 120% of the filament width,[13] whence the condition of the existence of parallel bordered filaments can be quantified.

It should be stressed that the macroscopically observable phenomenon of field redistribution towards a uniform state is a direct consequence of the constant critical field along the filament boundaries. The existence of this critical field can be deduced from analogy with phase transitions in equilibrium thermodynamics.[1] This was also confirmed by more complex physical model, based on microscopic generation-recombination kinetics.[15,16] Considering then the linear rela-

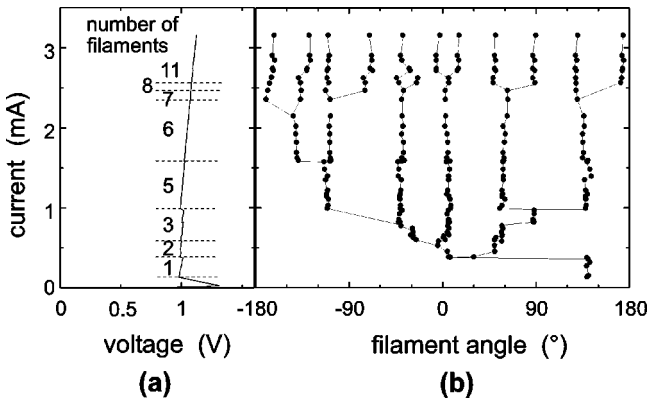

FIG. 4. (a) Current-voltage characteristic of a Corbino sample (C5) for a monotonically rising current (no hysteretic loops). (b) Angular orientations of the filaments, obtained from the photoluminescence pictures corresponding to the curve in (a).

tion between the length of a thin filament and the voltage drop along it, the critical field can be experimentally obtained from the holding voltage of the IV curve. Numerical values of $\mathcal{E}_c$ are shown in Table I.

Whereas the shape of the filaments does not depend on the chosen contact geometry, the way of generating multifilamentary patterns does. In the samples with concentric contact geometries filament splitting occurs at a critical width of a single filament and cannot be attributed to imperfections of the sample or contacts. Figure 4 shows the current-voltage characteristic of a Corbino sample and the angular orientations of filaments, obtained from photoluminescence pictures upon increasing the current. One sees that every splitting or rearrangement of the filaments is accompanied by a jump of the sample voltage in the order of 10 mV. The corresponding diagram of angular filament positions clearly reveals a bifurcation process. In contrast to the case of stripe contacts, the generation of each new filament in the Corbino samples originates from an elementary splitting process at a single filament, and not by the independent generation of additional filaments with rising current. However, a sequence of subsequent filament splittings is not reproducible, indicating a high degree of multistability of the system.[17]

More insight in the splitting behavior of filaments can be obtained by an inspection of a filament close to the division process. In Fig. 5(a) a parallel bordered filament is shown just before a splitting event. Upon slightly increasing the current it divides into two thinner filaments lying close to each other, Fig. 5(b); let us note that the fast dynamics of the splitting is not accessible by the present imaging technique. The arrangement of two closely neighboring filaments just after splitting is not quite stable. After a further increase of current or after a critical fluctuation the two filaments rearrange again to form an angle of about 45°, Fig. 5(c).

A possible mechanism for the filament splitting can be identified within the described model. In Fig. 5(d) the electric field strength is shown inside a Corbino sample with a single filament. It can be seen that in the vicinity of the outer electrode the filament gets broader, as the current lines end up normal to the metallic contact. Combined with the concave curvature of the outer contact this leads to a decrease of the field strength inside the filament, with the minimum on

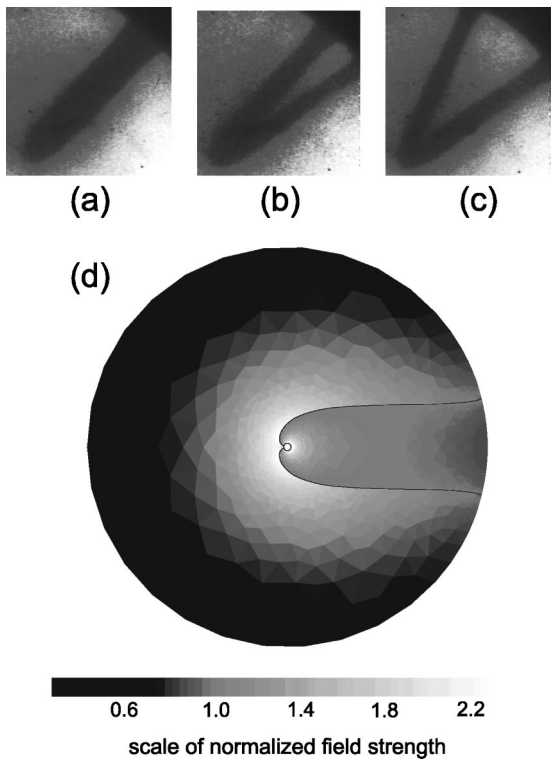

FIG. 5. Filament splitting process in a Corbino sample. (a) State just before the splitting, $I=0.898$ mA; (b) and (c) states after the splitting, $I=0.907$ mA (sample C5). (d) Numeric simulation of a filament in a Corbino sample. The gray scale of the field strength is stretched near the critical field to accent the field drop near the outer contact.

the filament axis. If this field minimum drops below the holding field of the high-conducting state, the arrangement becomes unstable and the splitting process starts from the unstable region.

The same mechanism of the filament splitting may hold for the ring geometry of the contacts. This is supported by the fact that in the Corbino sample with the diameter of the outer electrode of 2.1 mm the filament splitting has been observed at a filament width of 250 μm, whereas in the ring sample with an outer electrode diameter of 3 mm the critical width for the splitting has been 360 μm. The ratios of these critical widths to the respective diameters are the same in both cases, which indicates a scaled geometrical effect. According to the model, the minimum of the electric field for such a width-to-diameter ratio is equal to 92% of the critical field on the filament boundaries.

V. STABLE FILAMENT CONFIGURATIONS IN A MAGNETIC FIELD

Filamentary current flow reacts sensitively to a magnetic field applied perpendicularly to the epitaxial layer. A stationary filament configuration can either be destabilized, resulting in nonlinear voltage oscillations,[5,8,9,18,19] or it can be deformed, while the stability is preserved. In this article we restrict ourselves to the latter situation.

Figure 6 shows typical examples of stationary filament arrangements in the investigated contact geometries subject to a normal magnetic field at different currents. The fila-

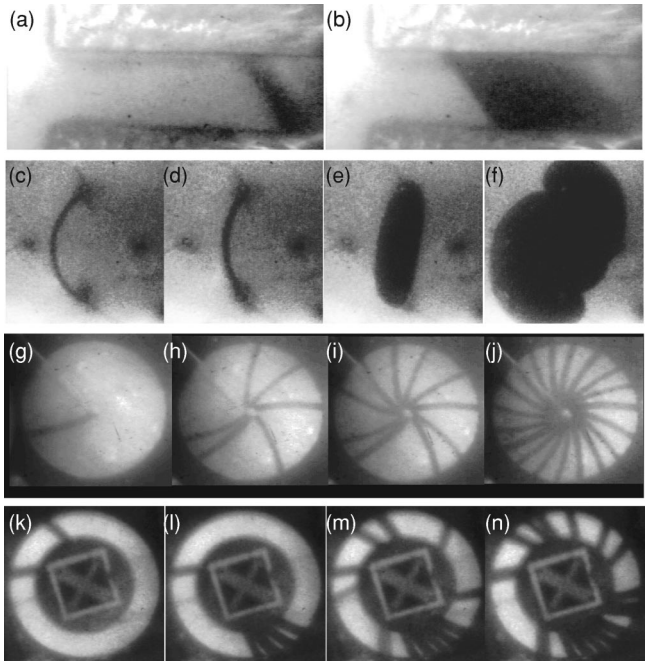

FIG. 6. Filament patterns in four different contact geometries in a normal magnetic field B: (a) and (b) parallel stripe contacts (sample PB01), $B=309$ mT, $I=1.17$, 3.82 mA; (c)–(f) two point contacts (sample PC06), $B=216$ mT, $I=0.26$, 0.33, 2.15, 12.1 mA; (g)–(j) Corbino geometry (sample C1), $B=152$ mT, $I=0.2$, 1.1, 1.7, 3.3 mA; (k)–(n) ring geometry (sample C6), $B=237$ mT, $I=0.7$, 1.9, 4.4, 5.9 mA.

ments between two parallel stripe contacts become tilted by an angle which increases monotonically with magnetic field strength B [Fig. 6(a)]. In contrast to its clear dependence on the magnetic field, the tilting angle remains almost unchanged with varying sample current, even if the current direction is inverted, Fig. 6(b).

In samples with two point contacts a stationary lateral displacement of thin stripelike filaments has been observed, Fig. 6(c). The filaments are always bent in the direction of the Lorentz force on the free electrons. Keeping the magnetic field constant the lateral displacement of the filament is reduced with increasing current, Fig. 6(d).

At higher currents, when the filament width is not negligible compared to its length, no distinct bending can be observed any more, Fig. 6(e). Increasing further the current the filament width becomes comparable to the contact distance and the situation changes qualitatively: the form of the filament becomes S-shaped and the filament borders near the contacts follow a spiral-like line.

In samples with concentric contact geometries [Figs. 6(g)–6(n)] the current flow in the magnetic field deviates clearly from the radial direction. The filament patterns become spiral in the case of Corbino samples, and waterwheel-like in the case of ring geometry.

The stripelike filament tilted by a constant angle between two parallel stripe contacts corresponds again to a trivial solution of the model. As can be seen from Eq. (1), the current lines run deflected by a Hall angle $\Theta_H=\arctan(\mu B)$ from the electric field vector. Consequently, every parallel bordered stripe of constant conductivity, which runs along this angle in the fixed electric field between wide parallel contacts, is a

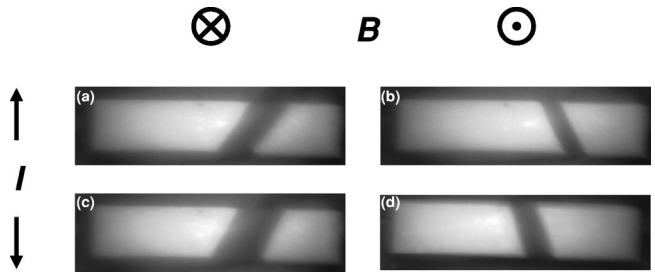

FIG. 7. Filament arrangement between two parallel stripe contacts for different orientations of current flow and magnetic field. (a)–(d): $I=1.21$, 0.73, -1.47, -1.01 mA, $B=-214$, 150, -150, 95 mT. (Sample PB15.)

solution of the problem. Filaments of this type thus allow the visual determination of the Hall angle for a given magnetic field.[20]

For further discussion it is helpful to look at the symmetry behavior of the filaments under inversion of current and magnetic field direction. In Fig. 7 all combinations of field orientations are shown for a filament between two parallel stripe contacts. It can be seen that only under an inversion of the magnetic field the tilting of the filament changes, whereas an inversion in the current flow direction does not lead to any change in the tilting of the filament. This result corresponds to a description of the current flow in the Drude theory: upon inverting B, the Hall angle changes its sign while the current orientation does not; upon inverting the direction of the current $\boldsymbol{j}$, the electric field $\boldsymbol{\mathcal{E}}$ is also inverted. Therefore, only the reference direction of the Hall angle is inverted; the angle between the filament and the contact remains the same. Hence, no change in the image can be observed.

The situation is more complex for filaments between two point contacts. In the case of a narrow filament, the filament is always displaced in the direction of the Lorentz force on the free carriers, and this direction inverts, if *either* the magnetic field *or* the current direction is inverted, as shown in Fig. 8(a). A simultaneous inversion of current and magnetic field orientation leads to almost no change of the filament pattern. The symmetry behavior changes qualitatively if one

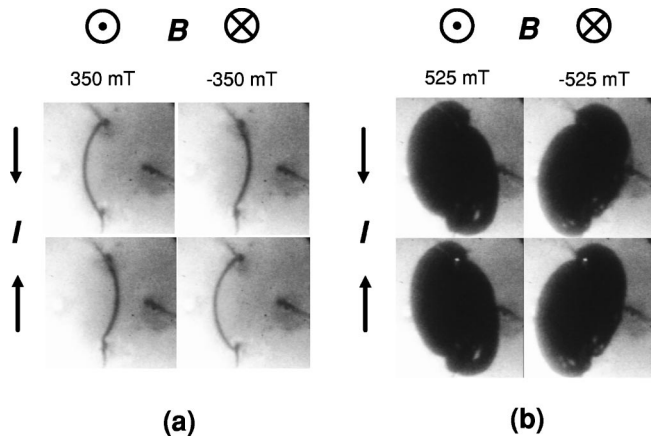

FIG. 8. Stationary filaments between two point contacts in a normal magnetic field for different directions of magnetic field and current. (a) Regime of thin low-current filaments, $I=0.3$ mA; (b) regime of thick high-current filaments, $I=11$ mA. (Sample PA06.)

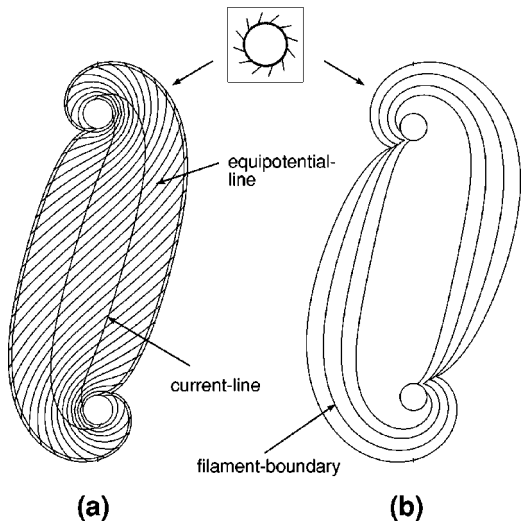

FIG. 9. Numerical simulation of S-shaped filaments between two point contacts. (a) Single filament with indicated current and equipotential lines, (b) boundary curves of four filaments at $\tan(\Theta_H)=1.6$ and various biases. In the inset the course of current lines near the contacts is illustrated.

looks at wide S-shaped filaments between two point contacts, as shown in Fig. 8(b). Here the filament shape inverts only under an inversion of the magnetic field but not under an inversion of the current direction, just as in the case of tilted stripelike filaments between parallel contacts as shown in Fig. 7.

Solutions of the model in the case of two point contacts are shown in Fig. 9. The agreement with the experiment is good in the case of wide, S-shaped filaments, but the model completely fails in the case of thin filaments. This is not surprising if we analyze the symmetry of the possible solutions of the above defined free-boundary problem. It turns out that given a valid solution $\boldsymbol{\mathcal{E}}(x,y)$ of the problem, the vector function $\boldsymbol{\mathcal{E}}'=\boldsymbol{\mathcal{E}}(-x,-y)$ is also a valid solution (if the sample geometry allows such a transformation), but functions $\boldsymbol{\mathcal{E}}'=\boldsymbol{\mathcal{E}}(x,-y)$ and $\boldsymbol{\mathcal{E}}'=\boldsymbol{\mathcal{E}}(-x,y)$ are not. In other words, every valid solution of a problem based on the Drude model exhibits the point symmetry with respect to the center of symmetry of the sample. This is the case for the S-formed filaments of Figs. 8(b) and 9, as well as for the stripelike filament of Fig. 7. On the other hand, the model is principally not capable to yield a solution of an approximate reflection symmetry, as observed with thin filaments displayed in Fig. 8(a).

To correctly model the bending of thin filaments, additional processes have to be taken into account going beyond the Drude model. They may relate directly to the motional effect of the Lorentz force associated with the electron momentum relaxation in the filament borders.[9] However, an indirect effect of the Lorentz force is probably more significant. It is connected with the stationary state equilibrium between the strong outward diffusion of free electrons through the filament boundary, and their drift back due to the local charge redistribution. In a magnetic field this delicate balance is likely to be disturbed, which results in an effective motion of the filament boundary. Independent of the exact mechanism, in both the above cases the Lorentz force effectively acts only on the filament edges, where significant gradients of system variables exist. In contrast to this ''edge effect,'' the ''Drude effect'' of the Lorentz force, manifested by the Hall angle, acts on a large spatial scale and also reflects the electrostatics of the contact geometry. Consequently, the transition from a thin bendable filament to a wide filament with point symmetry can be understood as a change of the relative importance of these two effects.

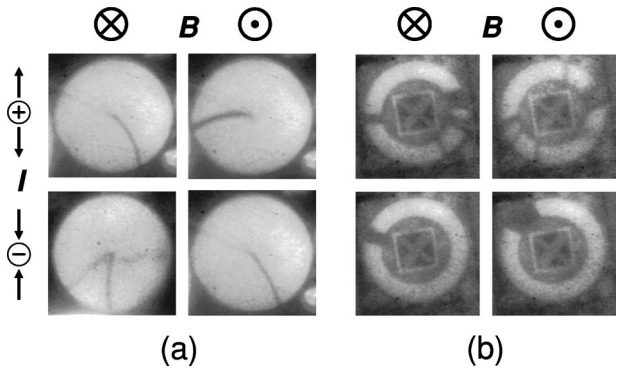

FIG. 10. Stationary filaments between two concentric contacts in a normal magnetic field for different directions of magnetic field and current. (a) Corbino disk (sample C5), (b) ring sample (C6). Currents and magnetic fields are (clockwise from upper left) (a) $I=0.11,\ 0.20,\ -0.11,\ -0.13$ mA, $B=-170,\ 170,\ 100,\ -77$ mT; (b) $I=2.29,\ 2.79,\ -1.71,\ -0.81$ mA, $B=-111,\ 183,\ 41,\ -41$ mT.

Figure 10 shows the symmetry behavior of filaments under an inversion of current or magnetic field direction for the case of concentric contacts. In the Corbino samples the filament bending changes orientation under an inversion of either current or magnetic field orientations. The situation is thus analogous to a thin filament between two point contacts. Let us note that this is in contrast to the well-known spiral curvature of the current lines in a uniformly conducting Corbino sample, which reverts only with the magnetic field. In the case of a ring-shaped sample one cannot make a clear statement of the symmetry behavior due to the loss of stability at higher magnetic fields.

The problem of the filament stability is encountered in both investigated concentric geometries. It turns out that stable filament arrangements can easily be found only for one bias polarity, with the cathode being on the outer electrode. At the reversed current direction stationary patterns can be found only in small islands of magnetic field and current in the case of Corbino samples, and for very low magnetic fields in the case of the ring samples. A probable explanation of this phenomenon is illustrated in Fig. 11.

The symmetry behavior of a filament in the Corbino sample implies the presence of a filament-pinning imperfection near the outer electrode, analogously to the case of two point contacts. The bending of such a pinned thin filament always occurs in the direction of the Lorentz force. The orientation of the filament bending determines the angle at which the filament merges into the outer electrode. However, the sign of this angle may differ from the sign of the Hall angle, which is formed by the current lines—i.e., the filament borders—and the equipotential of the outer contact. It can easily be seen that an agreement between the two angles occurs in the case of the electron conductivity with the negative pole on the outer electrode, Fig. 11(a), while with the

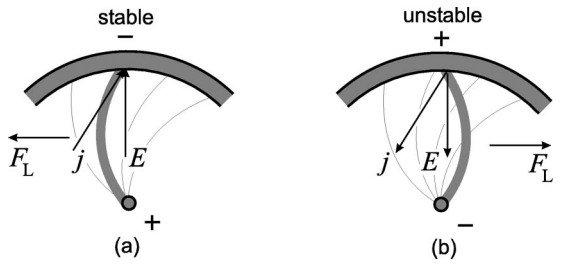

FIG. 11. Illustration of different effects of the filament bending (due to the edge-effect of the Lorentz force) and current-line tilting (due to the Drude-effect). In (a) the two relevant angles agree and a stable configuration is possible; in (b) the two angles disagree and the filament gets unstable.

reversed bias polarity the opposite sign is always realized independent of the magnetic field orientation. For holes the situation would be just the other way round.

VI. SUMMARY

Applying an optical technique it was possible to investigate the formation of the current pattern in the regime of low-temperature impurity breakdown in various contact arrangements. It was shown that independent of the chosen contact-geometry the shape of current filaments at nucleation is characterized by parallel running boundaries. This property of the filaments could be attributed to the constant critical field, which applies along the interface between the high- and low-conducting phases.

No characteristic length was found in the process of filament splitting between parallel contacts. The critical filament width for splitting in samples with concentric contacts was shown to scale linearly with the contact diameter, indicating a geometrical effect.

In a magnetic field normal to the plane of the semiconductor, thin filaments at low current levels were shown to be bent in the direction of the Lorentz force. The bending turns up in an S-shaped deformation for high currents. These two regimes demonstrate the different effects of the Lorentz force. Whereas in the case of thin filaments the Lorentz force influences primarily the filament boundaries, the wide S-shaped filaments are formed by the large scale Drude effect. A model based on the Drude theory has been constructed, which reproduces the regime of a thick filament in very good agreement with the experiment.

ACKNOWLEDGMENTS

The authors are indebted to E. Schöll for stimulating discussion and H. Kostial, M. Cukr, and J. Oswald for the sample preparation. Financial support by the Deutsche Forschungsgemeinschaft and the Alexander von Humboldt Foundation is gratefully acknowledged.

*Permanent address: Universität Münster, Institut für Angewandte Physik, Corrensstrasse 2/4, 48149 Münster, Germany.

[1] E. Schöll, *Nonequilibrium Phase Transitions in Semiconductors* (Springer-Verlag, Berlin, 1987).
[2] V. Novák, C. Wimmer, and W. Prettl, Phys. Rev. B **52**, 9023 (1995).
[3] W. Clauss, C. Muz, and W. Mueller, Z. Phys. B: Condens. Matter **102**, 553 (1997).
[4] K. Aoki, Phys. Status Solidi B **204**, 481 (1997).
[5] J. Spangler, B. Finger, C. Wimmer, W. Eberle, and W. Prettl, Semicond. Sci. Technol. **9**, 373 (1994).
[6] W. Eberle, J. Hirschinger, U. Margull, W. Prettl, V. Novák, and H. Kostial, Appl. Phys. Lett. **68**, 3329 (1996).
[7] V.V. Bel'kov, J. Hirschinger, V. Novák, F.-J. Niedernostheide, S.D. Ganichev, and W. Prettl, Nature (London) **397**, 398 (1999).
[8] *Nonlinear and Chaotic Transport Phenomena in Semiconductors*, edited by Y. Abe, special issue of Appl. Phys. A: Solids Surf. **48**(2), (1989).
[9] W. Clauss, U. Rau, J. Peinke, J. Parisi, A. Kittel, M. Bayerbach, and R. Huebener, J. Appl. Phys. **70**, 232 (1991).
[10] G. Hüpper, and E. Schöll, Phys. Rev. Lett. **66**, 2372 (1991).
[11] F.-J. Niedernostheide, J. Hirschinger, W. Prettl, V. Novák, and H. Kostial, Phys. Rev. B **58**, 4454 (1998).
[12] E.H.C. Parker, *The Technology and Physics of Molecular Beam Epitaxy* (Plenum, New York, 1985).
[13] V. Novák, J. Hischinger, W. Prettl, and F.-J. Niedernostheide, Semicond. Sci. Technol. **13**, 756 (1998) (note that the relaxation factor β relates to filament half-width).
[14] K.M. Mayer, R.P. Huebener, and U. Rau, J. Appl. Phys. **67**, 1412 (1990).
[15] M. Gaa, R.E. Kunz, and E. Schöll, Phys. Rev. B **53**, 15 971 (1996).
[16] K. Kunihiro, M. Gaa, and E. Schöll, Phys. Rev. B **55**, 2207 (1997).
[17] J. Hirschinger, W. Eberle, W. Prettl, F.-J. Niedernostheide, and H. Kostial, Phys. Lett. A **236**, 249 (1997).
[18] M. Hirsch, A. Kittel, and J. Parisi, Phys. Rev. B **54**, 13 734 (1996).
[19] W. Eberle, U. Margull, J. Grebler, J. Hirschinger, W. Prettl, H. Kostial, and V. Novák, Acta Tech. CSAV **42**, 623 (1997).
[20] V. Novák, J. Hirschinger, F.-J. Niedernostheide, W. Prettl, M. Cukr, and J. Oswald, Phys. Rev. B **58**, 13 099 (1998).